# Electronic Supplementary Information for *Strontium speciation in archaeological otoliths*

Phil K. Cook, Elise Dufour, Marie-Angélique Languille, Cristian Mocuta, Solenn Réguer, and Loïc Bertrand

## SI.1 Preparation of otolith sections

Polyester resin (Buehler) was used for HP-11, HP-12, GP-292, 111 and 424; epoxy resin (ref. K2020, Brot Technologies) was used for QCD, Bayovar-1C, and BH17. Embedded samples were then cut into frontal (sagittae) or transverse (lapilli) sections using a diamond disk or wire saw. Sections were then mounted to microscope slides using Crystalbond 509 (Structure Probe Inc., Paris, France) for QCD, Bayovar-1C, and BH17, or Brot D200 glue (Brot Technologies) for HP-11, HP-12, GP-292, 111 and 424. Sections were carefully polished using progressively finer grit, first by hand using 13 µm then 3 µm silicon carbide suspensions (Brot Technologies), finishing by polishing machine with a 0.1 µm alumina suspension (Brot Technologies) on a velvet disk (Escil, Chassieu, France). Gentle polishing did not prevent detachment of some crystals at the edge of *G. peruvianus* otoliths. Internal stresses during the preparation process can also induce cracks in some samples. *Micropogonias* sp., *G. peruvianus*, and *Cathorops* sp. otoliths are typically large (several millimetres) and exhibit growth increments on the order of up to a few hundred micrometres.[1,2]

## SI.2 Treatment of EXAFS spectra

Extrapolation of the edge jump and normalisation was performed using values in the pre-edge region, from 60–30 eV below the absorption edge ($E_0$), and in the post-edge region at 16–670 eV after $E_0$ region for µEXAFS. As oscillations extend in the whole XANES region, normalisation of XANES spectra was performed by adjusting the normalisation range to align the spectrum with similar EXAFS spectra from visual comparison. The data were normalised and post-edge region flattened using ATHENA[3] with a $E_0$ approximated at the energy corresponding to half of the edge jump. An arctangent function was fitted to the pre-edge region, defined as points of normalised intensity below 0.45 of the edge jump, and post-oscillation region, defined as $E \geq 16\,300$ eV. The $E_0$ determined from the fitted arctangent function was used for the rest of the treatment. Spectrum background was removed by fitting with splines over the full energy range after $E_0$, unless noted differently. In the processing of EXAFS data, a $k^2$-weighting was used to amplify the spectrum in the mid- to high-$k$ range without excessively weighting the noise in the upper $k$ range. A Hanning apodisation window from 1–9 $Å^{-1}$ with a taper of 1 $Å^{-1}$ was applied before applying a Fourier transform to retrieve the pseudo-radial distribution with phase correction from FEFF calculations on the first O shell. EXAFS fitting was performed on the interval 1–6 Å in R-space. Occupancy of each shell was fixed at theoretical values.

## SI.3 SEM Images of otoliths

Figures S1 to S3 present images of the *G. peruvianus* otoliths after an acid attack and carbon coating. Similar features are visible throughout both archaeological and modern samples, indicating that the microstructure is preserved.

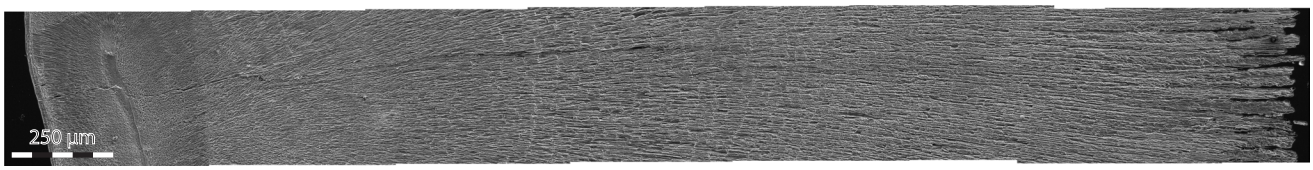


(a) Transect composite image

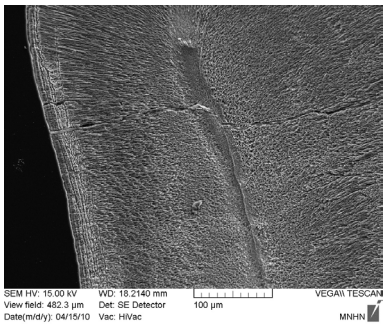


(b) Left edge

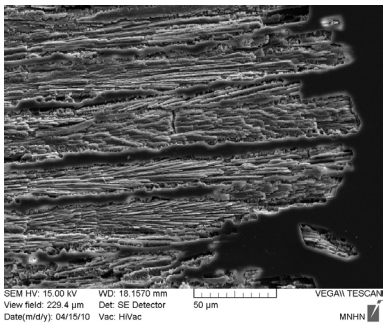


(c) Right edge

Figure S1: Secondary electron images of HP-11 (*G. peruvianus*, Huaca Prieta).

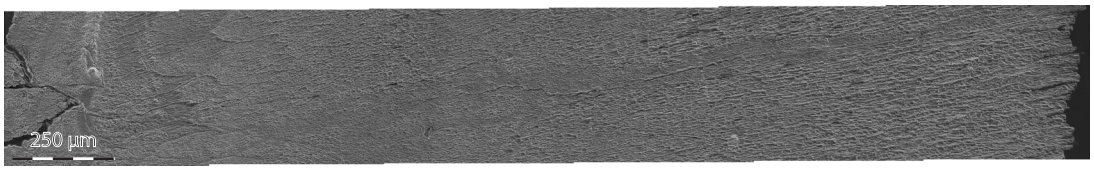


(a) Transect composite image

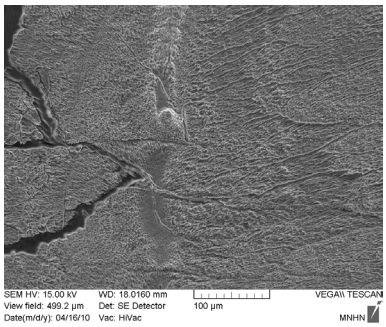


(b) Left edge

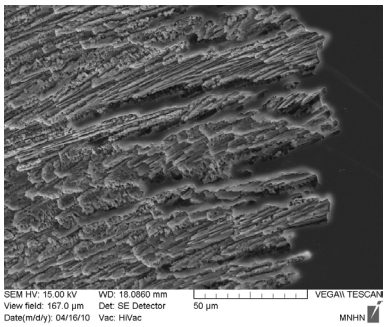


(c) Right edge

Figure S2: Secondary electron images of HP-12 (*G. peruvianus*, Huaca Prieta).

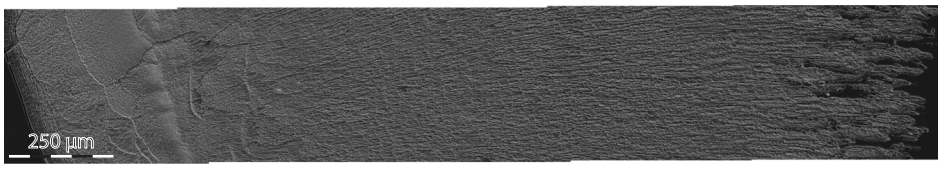


(a) Transect composite image

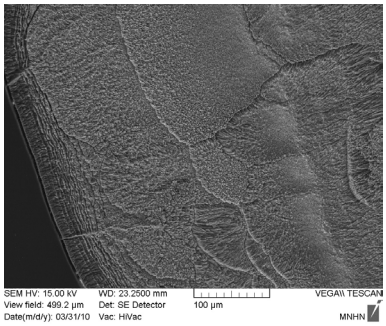


(b) Left edge

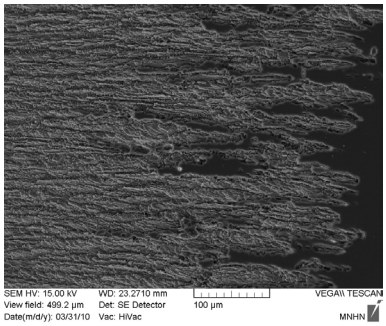


(c) Right edge

Figure S3: Secondary electron images of GP-292 (*G. peruvianus*).

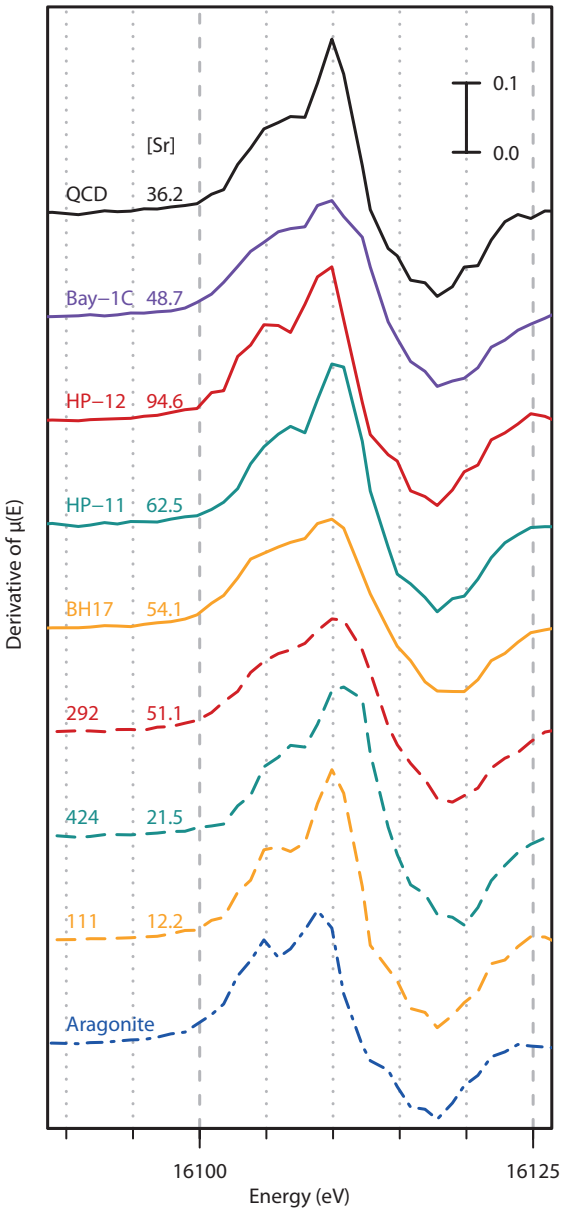


Figure S4: First derivatives of XANES spectra in Fig. 3b illustrating the multiple inflection points observed. Spectra have been vertically shifted.

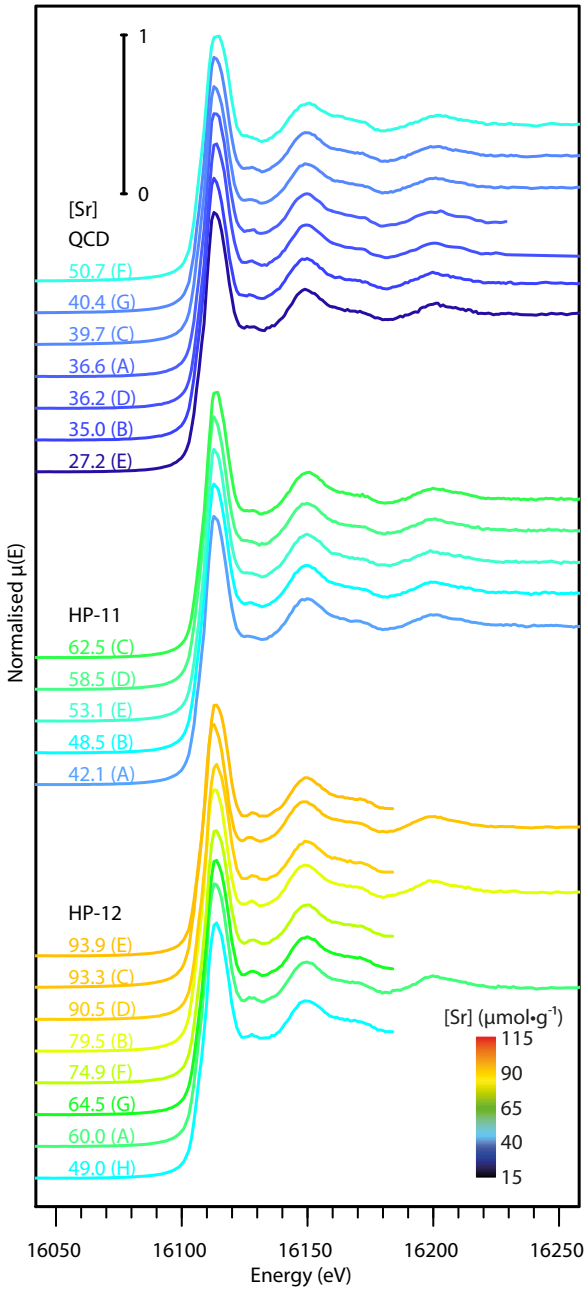


Figure S5: Comparison of µXANES spectra at Sr K-edge at varying Sr concentrations on the archaeological otoliths QCD (*Micropogonias* sp., Pampa de los fósiles, Peru), HP-11, and HP-12 (*G. peruvianus*, Huaca Prieta, Peru). The Sr content determined by µXRF is marked in $\mu mol \cdot g^{-1}$ above each curve. Spectra have been vertically shifted.

Table S1: Reference unit cell parameters of aragonite, strontianite, calcite, and vaterite[4–8]

| | Aragonite | Strontianite | Calcite | Vaterite |
|---|---|---|---|---|
| Ca coordination | 9 | 9 | 6 | 8 |
| System | Orthorhombic | Orthorhombic | Rhombohedral | Hexagonal |
| Space group | $Pmcn$ | $Pmcn$ | $R\bar{3}c$ | $P6_3/mmc$ |
| $a$ (Å) | 4.96183 (1) | 5.107 | 4.989 | 4.130 |
| $b$ (Å) | 7.96914 (2) | 8.414 | 4.989 | 4.130 |
| $c$ (Å) | 5.74285 (2) | 6.029 | 17.062 | 8.490 |
| $\alpha$ (°) | 90 | 90 | 90 | 90 |
| $\beta$ (°) | 90 | 90 | 90 | 90 |
| $\gamma$ (°) | 90 | 90 | 120 | 120 |
| Unit cell volume (Å$^3$) | 227.081 | 259.07 | 424.67 | 125.41 |

Table S2: EXAFS fitting results

| Sample | $R_{Sr\text{-}O}$ (Å) | $R_{Sr\text{-}C}$ (Å) | $R_{Sr\text{-}M}$ (Å) | $\sigma^2_{Sr\text{-}O}$ | $\sigma^2_{Sr\text{-}C}$ | $\sigma^2_{Sr\text{-}M}$ | $\Delta E_0$ (eV) |
|---|---|---|---|---|---|---|---|
| Aragonite | 2.565 ± 0.020 | 2.931 ± 0.087 | 3.980 ± 0.036 | 0.011 ± 0.002 | 0.041 ± 0.032 | 0.012 ± 0.004 | 4.201 ± 1.266 |
| Strontianite | 2.601 ± 0.015 | 2.982 ± 0.116 | 4.155 ± 0.042 | 0.011 ± 0.001 | 0.059 ± 0.047 | 0.010 ± 0.012 | 4.915 ± 1.404 |
| QCD | 2.579 ± 0.025 | 2.957 ± 0.141 | 3.975 ± 0.053 | 0.009 ± 0.002 | 0.046 ± 0.062 | 0.013 ± 0.006 | 4.201 ± 2.452 |
| HP-12 | 2.583 ± 0.026 | 3.01 ± 0.106 | 3.966 ± 0.053 | 0.009 ± 0.002 | 0.039 ± 0.046 | 0.013 ± 0.006 | 4.61 ± 2.255 |
| Bayovar-1C | 2.553 ± 0.027 | 2.854 ± 0.150 | 3.965 ± 0.057 | 0.013 ± 0.004 | 0.031 ± 0.032 | 0.016 ± 0.007 | 3.81 ± 2.340 |
| BH17 | 2.571 ± 0.023 | 2.958 ± 0.099 | 3.984 ± 0.048 | 0.011 ± 0.002 | 0.037 ± 0.037 | 0.014 ± 0.014 | 5.039 ± 2.021 |
| 424 | 2.584 ± 0.024 | 2.983 ± 0.100 | 3.983 ± 0.055 | 0.009 ± 0.002 | 0.037 ± 0.040 | 0.015 ± 0.067 | 5.039 ± 2.067 |
| 111 | 2.568 ± 0.034 | 2.933 ± 0.074 | 3.963 ± 0.068 | 0.010 ± 0.003 | 0.030 ± 0.029 | 0.013 ± 0.008 | 4.201 ± 1.257 |
| GP-292 | 2.583 ± 0.021 | 2.971 ± 0.076 | 3.988 ± 0.044 | 0.010 ± 0.002 | 0.030 ± 0.024 | 0.015 ± 0.006 | 5.720 ± 1.611 |

## References


[1] P. Béarez, G. Carlier, J. Lorand and G. Parodi, *Comptes Rendus Biologies*, 2005, **328**, 243–252.

[2] P. Béarez, E. Dufour, J. Crédou and C. Chauchat, in *Peuplements et préhistoire en Amériques*, ed. D. Vialou, CTHS, 2011, pp. 233–246.

[3] B. Ravel and M. Newville, *Journal of Synchrotron Radiation*, 2005, **12**, 537–541.

[4] E. Caspi, B. Pokroy, P. Lee, J. Quintana and E. Zolotoyabko, *Acta Crystallographica Section B-Structural Science*, 2005, **61**, 129–132.

[5] H. Swanson and R. Fuyat, *Circular of the Bureau of Standards: Standard X-ray diffraction powder patterns*, National Bureau of Standards, 1953.

[6] S. R. Kamhi, *Acta Crystallographica*, 1963, **16**, 770–772.

[7] R. L. Sass, R. Vidale and J. Donohue, *Acta Crystallographica*, 1957, **10**, 567–570.

[8] S. Hayakawa, Y. Hajima, S. Qiao, H. Namatame and T. Hirokawa, *Analytical Sciences*, 2008, **24**, 835–837.